NAWCWD TP 8460

An Electrically Small Switchable Chaotic Dipole Antenna

by
P. L. Overfelt
D. J. White
Physics and Computational Sciences Division
Research Department

FEBRUARY 2000

NAVAL AIR WARFARE CENTER WEAPONS DIVISION
CHINA LAKE, CA 93555-6100

Approved for public release; distribution is unlimited.

Naval Air Warfare Center Weapons Division

FOREWORD

This report documents work carried out and completed during fiscal years 1999 and 2000 under the In-House Laboratory Independent Research Program. This research resulted in a theoretical analysis of a nonlinear antenna that could switch in operation between periodic and chaotic radiated behavior.

Approved by
J. FISCHER, Head
Research Department
21 March 2000

Under authority of
C. H. JOHNSTON
Capt., U.S. Navy
Commander

Released for publication by
K. HIGGINS
Director for Research and Engineering

NAWCWD Technical Publication 8460

Published by ..... Technical Information Division
Collation ..... Cover, 13 leaves
First printing ..... 45 copies

REPORT DOCUMENTATION PAGE

Form Approved
OMB No. 0704-0188

1. AGENCY USE ONLY *(Leave blank)*	2. REPORT DATE	3. REPORT TYPE AND DATES COVERED
	February 2000	Final, FY99-00

4. TITLE AND SUBTITLE
An Electrically Small Switchable Chaotic Dipole Antenna (U)

5. FUNDING NUMBERS

6. AUTHOR(S)
P. L. Overfelt, D. J. White

7. PERFORMING ORGANIZATION NAME(S) AND ADDRESS(ES)
Naval Air Warfare Center Weapons Division
China Lake, CA

8. PERFORMING ORGANIZATION REPORT NUMBER
NAWCWD TP 8460

9. SPONSORING/MONITORING AGENCY NAME(S) AND ADDRESS(ES)

10. SPONSORING/MONITORING AGENCY REPORT NUMBER

11. SUPPLEMENTARY NOTES

12a. DISTRIBUTION/AVAILABILITY STATEMENT
Approved for public release; distribution is unlimited.

12b. DISTRIBUTION CODE

13. ABSTRACT *(Maximum 200 words)*

(U) An electrically small dipole antenna loaded with Chua's oscillator as a nonlinear load is analyzed. By using certain values for the linear reactive and resistive elements of this circuit, various types of periodic, period-doubled, and chaotic behavior that occurs for the voltage at the antenna input terminals is shown to occur also for the associated radiated electromagnetic field components. Using three cases, i.e., periodic, period-4, and chaotic behavior, the voltage characteristic dynamics determined at the input terminals are shown to be the same dynamics as those of the radiated electromagnetic field components. For an electrically small dipole, when the antenna voltage function is temporally chaotic, the antenna is demonstrated numerically to radiate temporally chaotic electromagnetic fields with the same dynamical behavior referenced to some later time also. Similarly, when the antenna voltage is periodic, the radiated fields will be periodically referenced to some later time. Switching between a periodic and a chaotic temporal electromagnetic field behavior is demonstrated to be possible by simply increasing the conductance of a single resistor of the antenna/Chua's oscillator equivalent circuit.

14. SUBJECT TERMS
Chua's oscillator, nonlinear antennas, chaotic antennas, chaotic electromagnetic fields

15. NUMBER OF PAGES
24

16. PRICE CODE

17. SECURITY CLASSIFICATION OF REPORT	18. SECURITY CLASSIFICATION OF THIS PAGE	19. SECURITY CLASSIFICATION OF ABSTRACT	20. LIMITATION OF ABSTRACT
UNCLASSIFIED	UNCLASSIFIED	UNCLASSIFIED	UL

CONTENTS

Figures:

ACKNOWLEDGEMENT

The authors thank Dr. Peter Kennedy of the University College Dublin, Dublin, Ireland, for the generous use of his ABC software.

1. INTRODUCTION

Since the early 1970s, many different techniques have been used to analyze the behavior of an antenna with a nonlinear load (References 1 through 11). While the characteristics of antennas with nonlinear loads have been analyzed in both the frequency and time domains, until now little attention has been given to possible chaotic effects that can result as a consequence of such nonlinearities. This oversight is not surprising, since only recently the field of chaos has moved from an essentially academic phenomenon to an intense applied research area in which chaotic behavior can be used to solve challenging technical problems.

In the following discussion, an electrically small dipole antenna was loaded with the nonlinear circuit known as Chua's circuit (References 12 through 17). A particularly simple and very widely studied real nonlinear dynamical system, Chua's circuit has a number of significant advantages over other similar nonlinear circuits. First, it is the simplest circuit known (consisting of a linear inductance, a linear resistance, two linear capacitances, and only one nonlinear element) that still exhibits a rich variety of chaotic phenomena. Second, it is a physical system for which the presence of chaos has been proven analytically, simulated numerically, and demonstrated experimentally (References 14 and 17). Third, Chua's circuit is easily constructed using standard electronic components at low cost (Reference 18). It is an ideal example of a low-order physically simple system that can exhibit extremely complex, nonperiodic, bounded behavior.

The reason for loading a dipole with Chua's circuit is to attempt to create an antenna that can easily switch from chaotic to nonchaotic behavior and vice versa. As is shown, this switching is easy to do in terms of the input voltage and current, as functions of time at the antenna input terminals, by simply changing certain values of the linear reactive and resistive elements (i.e., using variable resistors) that make up Chua's circuit. For an electrically small antenna (small in spatial extent such that the antenna length is only a small fraction of the wavelengths considered), it can be demonstrated numerically that when the antenna voltage function is temporally chaotic with a characteristic dynamical behavior the antenna will radiate temporally chaotic electromagnetic fields (referenced to some later time), exhibiting the same characteristic dynamical behavior. Similarly when the antenna voltage function is not chaotic, the associated fields (referenced to some later time) will be nonchaotic also. The ability to radiate a waveform that is predictable and periodic in time and then to suddenly switch to radiating a waveform that is complex and nonperiodic in time has obvious application to the area of secure communication.

In Section 2, the simplest equivalent circuit model for the electrically small dipole, modeled as a pure capacitance and loaded with a modification of Chua's circuit, known as Chua's oscillator, is shown and discussed. In Section 3, the relationship is derived between the voltages and currents resulting from the nonlinear load and the current that flows on the antenna element. Also an approximate vector potential function is introduced (based on the electrically small assumption) and the electromagnetic field components are determined. At this point both time series plots and delay coordinate plots of the electromagnetic field components are used to demonstrate when the electromagnetic fields are chaotic and when they are not. Section 4 provides discussion and conclusions.

2. EQUIVALENT CIRCUIT OF A SMALL DIPOLE LOADED WITH CHUA'S OSCILLATOR: ANTENNA CAPACITANCE

The original isolated Chua's oscillator, shown in Figure 1, is composed of two linear resistors, R = 1/G and R_0; two linear capacitances, C_1 and C_2; a linear inductor, L; and a voltage-controlled nonlinear resistor, N_R, called a Chua's diode (Reference 18). When R_0 is set equal to zero, this circuit is known as Chua's circuit. Figure 2 shows the electric dipole loaded with Chua's oscillator. Imposing the restriction that the antenna is thin and electrically small and can be modeled as an induced voltage, $V_a(t)$, at the antenna terminals and an antenna capacitance, C_a, (Reference 1), the antenna parameters and Chua's oscillator can be combined as in the equivalent circuit of Figure 3. In Figure 3, V_a and C_a are now in parallel with C_2, V_2 and C_1, V_1. This equivalent circuit results in three coupled ordinary differential equations given by

$$\dot{I}_3 = -\frac{1}{L}(R_0 I_3 + V_a) \tag{1a}$$

$$\dot{V}_a = \frac{1}{C_2 + C_a}\left[I_3 - (V_a - V_1)G\right] \tag{1b}$$

$$\dot{V}_1 = \frac{1}{C_1}\left[(V_a - V_1)G - f(V_1)\right] \tag{1c}$$

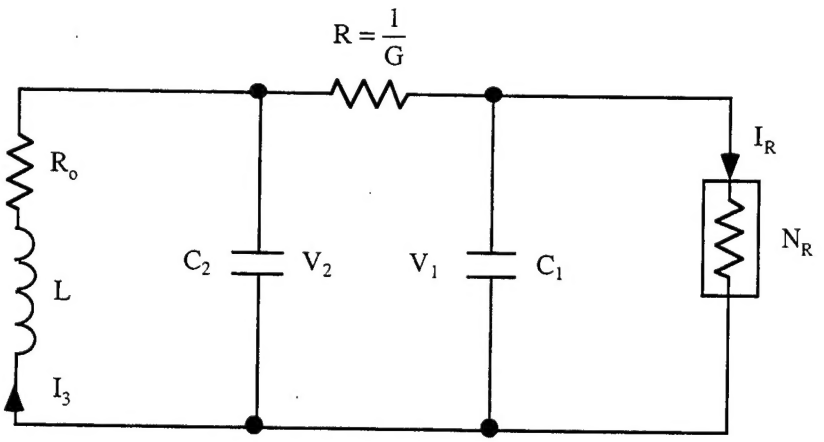

FIGURE 1. Chua's Oscillator.

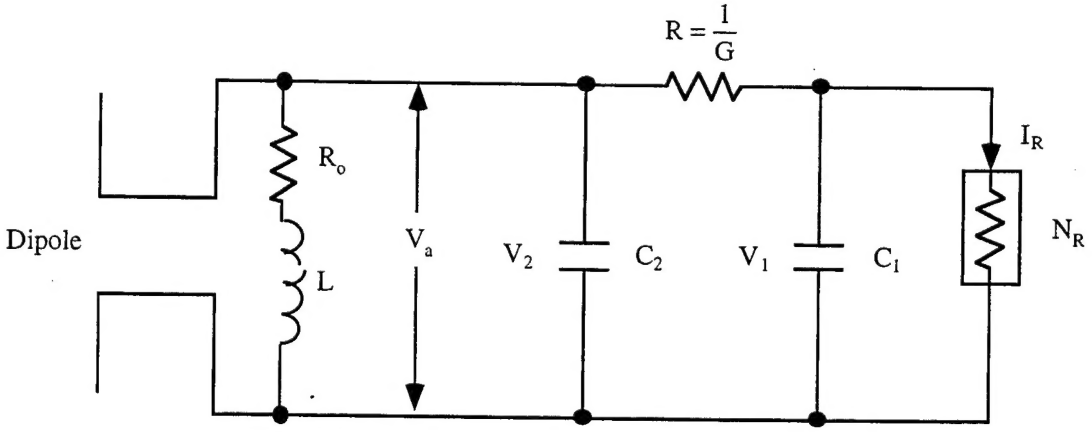

FIGURE 2. Nonlinearly Loaded Dipole Antenna.

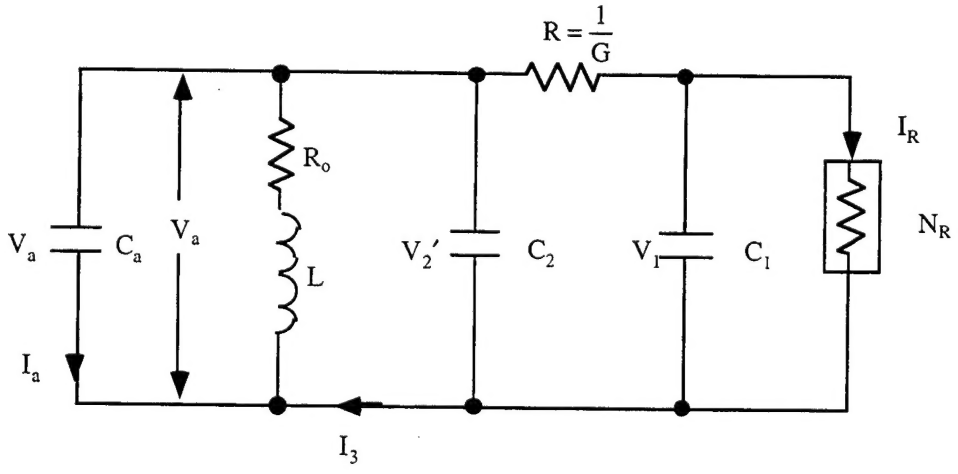

FIGURE 3. Equivalent Circuit of a Small Dipole Antenna Loaded With Chua's Oscillator.

Equation 1 describes a three-dimensional phase space (or state space) given by

$$\bar{X}(t) = \{I_3(t), V_a(t), V_1(t)\} \tag{2}$$

which is the state of the system at time t. A solution $\bar{X}(t)$ starting from some initial state, $\{I_3(t_0), V_a(t_0), V_1(t_0)\}$, at some beginning time, t_0, is called a trajectory of Equation 1. In Equation 1c, $f(V_1)$ denotes the piecewise-continuous linear approximation of the driving-point characteristic of the Chua's diode. The function $f(V_1)$ is given by Reference 17,

$$f(V_1) = \begin{cases} G_b V_1 + (G_b - G_a)E & ; \quad V_1 < -E \\ G_a V_1 & ; \quad V_1 < |E| \\ G_b V_1 - (G_b - G_a)E & ; \quad V_1 > E \end{cases} \tag{3}$$

where $E > 0$, $G_a < 0$, and $G_b < 0$ (Reference 17, Figure 3).

Several explanatory remarks are in order. In Figure 3, we used the fact that $V_a = V_2'$. Also it is important to note that the antenna capacitance, C_a, is usually on the order of 10^{-12} farads (F) for an electrically short thin dipole. This value is generally much less than typical values of C_2 (see Figure 3), which are usually on the order of 10^{-7} F (Reference 19). Thus, in general $C_a << C_2$ and $C_a << C_1$ also. From further consideration of Equations 1 and 3, if the C_2 of Figure 3 is reduced by the exact amount, C_a, then, when C_a is added back again into Equation 1, this three-dimensional system is numerically identical to the isolated Chua's oscillator equations. An analysis of this set of equations is given in Reference 19.

Once $V_a(t)$, the voltage at the antenna input terminals, is known from solution of Equation 1, the current on the antenna at the input terminals is given by

$$I_a(t) = C_a \dot{V}_a(t) \tag{4}$$

or

$$I_a(t) = \frac{C_a}{C_a + C_2}\{I_3(t) - [V_a(t) - V_1(t)]G\} \tag{5}$$

For the dynamical system of Figure 3, the three local Lyapunov exponents are given by

$$\lambda_1 = -\frac{R_0}{L} \tag{6a}$$

$$\lambda_2 = -\frac{G}{C_a + C_2} \tag{6b}$$

$$\lambda_3 = \begin{cases} -\dfrac{(G+G_b)}{C_1} & ; \text{ outer regions} \\ -\dfrac{(G+G_a)}{C_1} & ; \text{ inner region} \end{cases} \tag{6c}$$

It is obvious that λ_3 is the only local Lyapunov exponent with the possibility of being positive (and thus producing chaotic behavior) (References 20 and 21) in an average sense. The sign of λ_3 is, of course, dependent on the magnitude relationships among the linear conductances G, G_a, and G_b. Using Equation 1, and either Equation 4 or 5, the antenna current and voltage at the input terminals are known numerically as functions of time and are used in the next section to obtain the electromagnetic fields of the dipole antenna loaded with Chua's oscillator.

3. VECTOR POTENTIAL FORMULATION

Assuming that the small dipole of length 2h is oriented along the z-axis of a right-handed coordinate system, the associated vector potential can be written as

$$\vec{A}(\vec{r},t) = \hat{z}\frac{\mu_o}{4\pi}\int_{-h}^{h} \frac{I_a\left(z', t - \dfrac{|\vec{r} - z'\hat{z}|}{c}dz'\right)}{|\vec{r} - z'\hat{z}|} \tag{7}$$

At this point, if the antenna is small, one can assume that the current does not vary spatially along its length, z′. This is essentially an infinitesimal dipole assumption when the current is assumed to be constant in a spatial sense. (A triangular or sinusoidal spatial distribution could be used also if desired.) In this case,

$$I_a\left(z', t - \frac{|\vec{r} - z'\hat{z}|}{c}\right) \approx I_a\left(t - \frac{|\vec{r} - z'\hat{z}|}{c}\right) \tag{8}$$

For an electrically small antenna, the first-order approximation

$$\bar{r} \approx \bar{r} - z'\hat{z} \tag{9}$$

can be used, and thus the right-hand side of Equation 8 becomes

$$I_a\left(t - \frac{|\bar{r} - z'\hat{z}|}{c}\right) \approx I_a\left(t - \frac{r}{c}\right) \tag{10}$$

Now that Equation 10 can be used to replace the current function in Equation 7 and is no longer dependent on z′, the vector potential becomes simply

$$\bar{A}(\bar{r},t) \approx \hat{z}\frac{\mu_0(2h)}{4\pi} I_a\left(t - \frac{r}{c}\right) \tag{11}$$

Now, $I_a(t)$ is already known from solving Equation 1 numerically and subsequently substituting the results into either Equation 4 or 5, and thus the time-retarded function in Equation 11 is obtained by substituting the new argument, $t - \frac{r}{c}$, into the known $I_a(t)$. The new retarded time, $t' = t - \frac{r}{c}$, is simply an indication that as the dipole radiation moves outward in a spherical wave (at least, in the far-field) traveling at the speed of light, the radiation at time t′ will not reach some fixed field point, $\bar{r}$, until some later time, t.

Using

$$\bar{H} = \frac{1}{\mu_0}\nabla \times \bar{A} \quad ; \quad \frac{\partial \bar{E}}{\partial t} = c^2 \nabla \times \nabla \times \bar{A} \tag{12}$$

the electromagnetic field components in the time domain at some field point, $\bar{r}$, and some time, t, can be written in the form

$$H_\phi(\bar{r},t) = \frac{C_a h \sin\theta}{2\pi r}\left[\frac{1}{r}\frac{dV_a(t')}{dt'} + \frac{1}{c}\frac{d^2V_a(t')}{dt'^2}\right] \tag{13a}$$

$$E_r(\bar{r},t) = \frac{C_a h \cos\theta}{\varepsilon_0 \pi r^2}\left[\frac{V_a(t')}{r} + \frac{1}{c}\frac{dV_a(t')}{dt'}\right] \tag{13b}$$

$$E_\theta(\bar{r},t) = \frac{C_a h \sin\theta}{\varepsilon_0 2\pi r}\left[\frac{1}{rc}\frac{dV_a(t')}{dt'} + \frac{V_a(t')}{r^2} + \frac{1}{c^2}\frac{d^2V_a(t')}{dt'^2}\right] \tag{13c}$$

Equation 13b and c was obtained by substituting Equation 4 into Equations 11 and 12 and integrating indefinitely over the retarded time, t'. For now, the constants of integration have been set to zero for convenience. It is worth noting that in computing Equation 13, extensive use was made of the relationship

$$\frac{\partial I_a(t')}{\partial r} = -\frac{1}{c}\frac{\partial I_a(t')}{\partial t} = -\frac{1}{c}\frac{dI_a(t')}{dt'} \tag{14}$$

Because the electromagnetic field components in Equation 13 can all be expressed in terms of $V_a(t')$ and its time derivatives, we speculate that if the antenna is sufficiently small for the equivalent circuit model of Figure 3 to be accurate and if the antenna input voltage is chaotic then the electromagnetic field components will be temporally chaotic also (at some later time). Similarly, if $V_a(t')$ is not chaotic, then the fields will not be chaotic at some later time.

At this point it is necessary to demonstrate this translation of chaotic (or nonchaotic) behavior from the surface of the antenna, i.e., from the input terminals to the radiated electromagnetic field components. Usually time series plots of the electromagnetic field components (i.e., the field component amplitude plotted as a function of time) can be used. When a time series plot exhibits periodic behavior, the demonstration of periodicity is very compelling. However, chaotic states are not as easily shown to be chaotic simply from using time series plots. For possible chaotic states, it is more useful to employ a delay coordinate plot (Reference 22), which can reveal the characteristic shape of a chaotic attractor, if one exists. Thus, in Section 2 for $\bar{X}(t)$ given in Equation 2, it is possible to plot I_3, V_a, and V_1 in a three-dimensional state space and to determine whether I_3, V_a, and V_1 exhibit chaotic behavior. Each variable could also have been plotted as a function of time in a time series, although this method would not have been as effective for demonstrating chaos.

For the electromagnetic field components in Equation 13, these are known only as functions of time and can be plotted in time series also. But the delay coordinate method, for example, plots $E_\theta(\bar{r},t)$ vs. $E_\theta\left(\bar{r},t-\frac{r}{c}\right)$ vs. $E_\theta\left(\bar{r},t-\frac{2r}{c}\right)$. In this case, each value of some time series, i.e., $E_\theta(\bar{r},t)$ vs. t, is plotted versus a time-delayed version of itself. If the delay coordinate plot closes on itself, i.e., if the orbits are closed orbits, then periodic behavior has been demonstrated. If the delay coordinate plot is very complex, not closing on itself and producing some type of strange attractor, then chaotic behavior has been demonstrated. Although delay coordinates are generally used to reconstruct an initially unknown state space from a limited set of measured data, they can also be used for functions such as Equation 13.

To demonstrate numerically whether or not a chaotic (or periodic) voltage and current on the antenna will produce the same type of chaotic (or periodic) electromagnetic field behavior, three cases are considered:

1. A periodic antenna input terminal voltage, $V_a(t')$, is used where the conductance, $G = \frac{1}{R}$, in Figure 3 is 530.0 microsiemens (μS). (All other values are given in the figure legends.)

2. An antenna input terminal voltage, $V_a(t')$, is a limit cycle of period-four, obtained when the conductance is increased to 539.0 μS.

3. A fully chaotic antenna input terminal voltage, $V_a(t')$, is a spiral Chua's chaotic attractor, obtained when the conductance is increased to 550.0 μS.

Thus, the route to chaos that has been chosen is the period-doubling route and the bifurcation parameter is G, the conductance (References 19 and 21). We demonstrate numerically, using both time series plots and delay coordinate plots, that the dynamics occurring at the surface of the antenna also occur at some later time in the radiated electromagnetic field.

CASE 1: PERIODIC CASE

The first case assumes that the linear circuit parameters of the equivalent circuit in Figure 3 have values such that $V_a(t')$ is periodic (Reference 19) (Figure 4a). Figure 4a is a three-dimensional phase space plot of I_3, V_a, and V_1, determined by solving Equation 1. This plot is a limit cycle of period-1 and exhibits only one closed loop, immediately indicating the periodic nature of $V_a(t')$ in this case. Note that all circuit parameters are given in the figure captions. Figure 4b is the corresponding time series plot of the antenna voltage amplitude versus time and is oscillatory with a single period.

Figure 5a is a three-dimensional delay coordinate plot of the magnetic field, H_ϕ, at three separate times and separate fixed radii. Using Equation 13 and the extra parameters shown in Figure 5a, $H_\phi(t)$ vs. $H_\phi\left(t-\frac{r}{c}\right)$ vs. $H_\phi\left(t-\frac{2r}{c}\right)$ is plotted, where r is the radial distance to some field point away from the antenna and c is the speed of light. This delay coordinate plot of H_ϕ, while somewhat different in shape and orientation from the antenna voltage in Figure 4a, exhibits exactly the same dynamical behavior, i.e., a limit cycle of period-one.

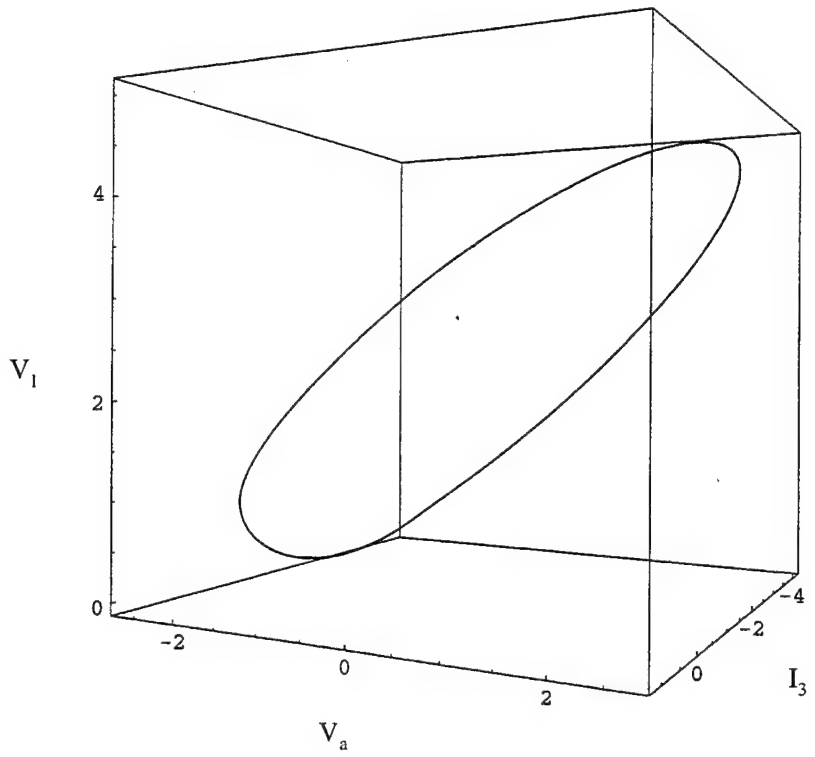

(a) Three-dimensional phase space plot of antenna voltage versus V_1 and I_3. Circuit parameters are R_0 = 12.5 Ω, L = 18.0 mH, C_1 = 10.0 nF, C_2 = 100.0 nF, G_a = -757.576 μS, G_b = -409.090 μS, E = 1.0 V, C_a = 10.0 pF, G = 530.0 μS.

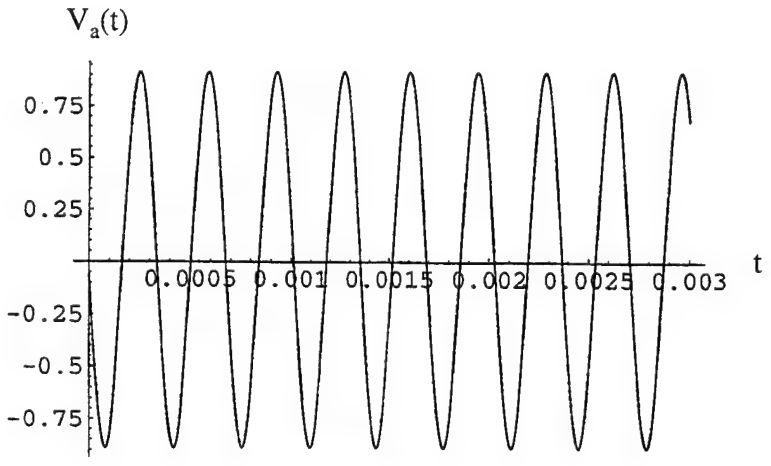

(b) Time series plot (same circuit parameters as Figure 4a).

FIGURE 4. Plot of Antenna Voltage Showing Periodic Behavior.

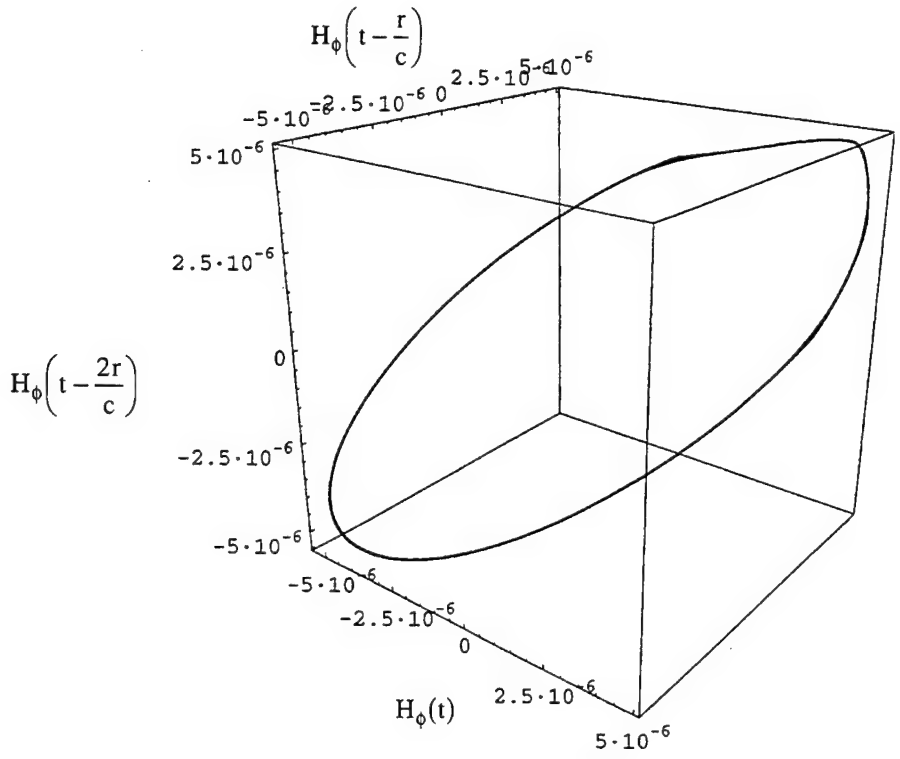

(a) Three-dimensional delay coordinate plot, H_ϕ. Circuit parameters are $R_0 = 12.5\ \Omega$, $L = 18.0$ mH, $C_1 = 10.0$ nF, $C_2 = 100.0$ nF, $G_a = -757.576\ \mu$S, $G_b = -409.090\ \mu$S, $E = 1.0$ V, $C_a = 10.0$ pF, $G = 530.0\ \mu$S, $r = 7.5 \times 10^3$ m, $h = 0.01$ m, $\theta = \pi/2$, $I_0 = 100$ A, $c = 3 \times 10^8$ m/s.

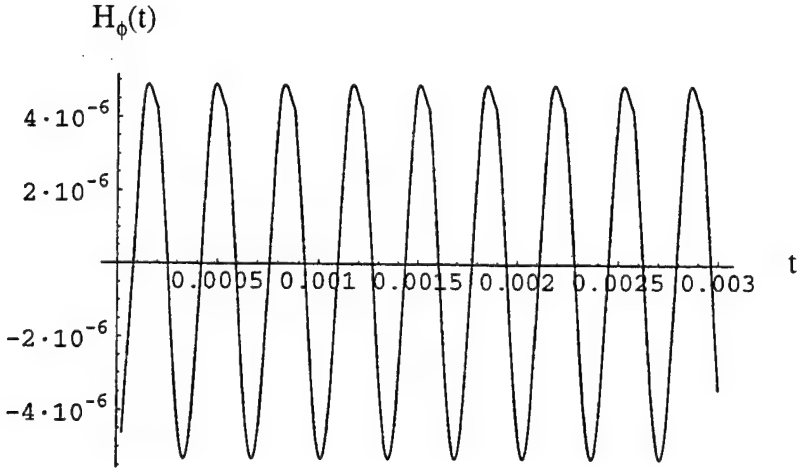

(b) Time series plot of magnetic field versus time (same parameters as Figure 5a).

FIGURE 5. Plot of Magnetic Field Showing Periodic Behavior.

In Figure 5b, the periodic nature of the magnetic field as a function of time, is shown in a time series plot. Similarly, Figure 6a is a three-dimensional delay coordinate plot of the electric field E_θ (since θ is assumed to be $\frac{\pi}{2}$, the E_r component is zero), at three separate times and separate fixed radii, i.e., $E_\theta(t)$ vs. $E_\theta\left(t-\frac{r}{c}\right)$ vs. $E_\theta\left(t-\frac{2r}{c}\right)$. It too exhibits period-one limit cycle behavior just as shown in Figure 4a. Figure 6b is the corresponding time series plot for E_θ as a function of time and is periodic.

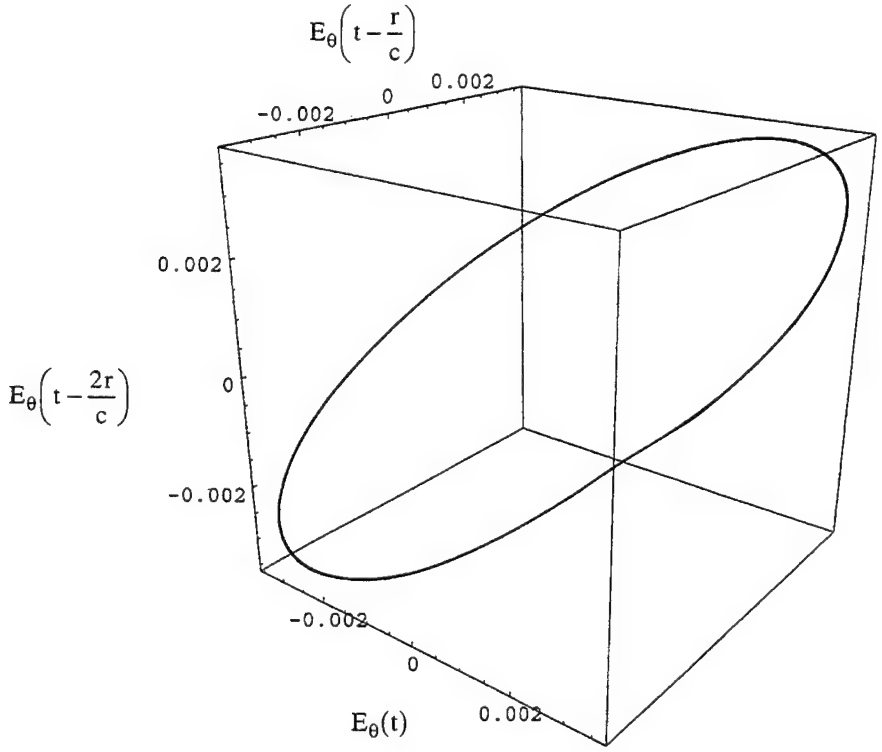

(a) Three-dimensional delay coordinate plot, E_θ, (same parameters as Figure 5a).

FIGURE 6. Plot of Electric Field Showing Periodic Behavior.

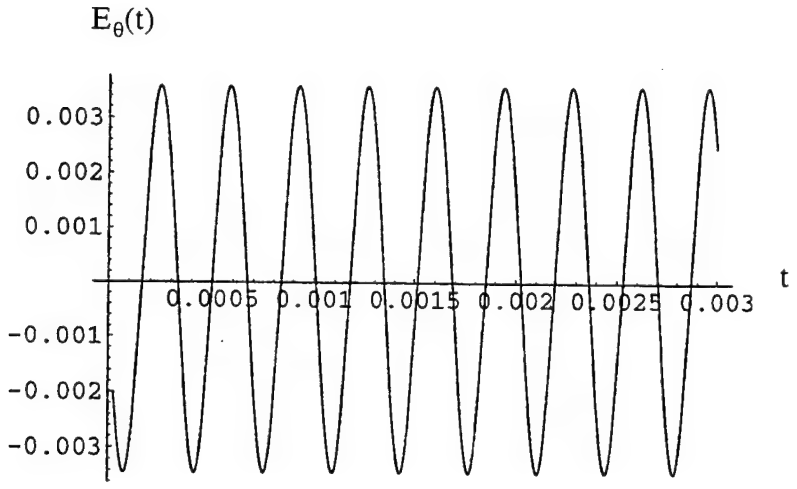

(b) Time series plot of electric field versus time (same parameters as Figure 5a).

FIGURE 6. (Contd.)

CASE 2: PERIOD-4 CASE

The second case assumes that the parameters of the equivalent circuit in Figure 3 are the same as in Case 1, with the exception that now G = 539 μS. Increasing the value of the conductance causes the limit cycle of Case 1 to now bifurcate so that it closes on itself after four loops of the trajectory. This is a result of period-doubling, a well known route to chaos (References 19, 21, and 22). This intermediate case is shown in Figure 7a, where the phase space dynamics involving the antenna voltage, V_a, exhibit four loops before closing on itself, indicating period-4 limit cycle behavior. The four distinct periods are also shown in the time series plot of V_a versus t in Figure 7b.

Using the same parameters as those used in Figure 7a, Figure 8a is a three-dimensional delay coordinate plot of the magnetic field, which also shows four separate loops indicating period-4 behavior. Although amplitude, orientation, and loop shape are different from those in Figure 7a, the period-4 dynamics are undeniable. Figure 8b is the corresponding time series plot with four distinct periods. Similarly in Figure 9a and b, the delay plot and the time series plot for E_θ exhibit the same period-4 behavior.

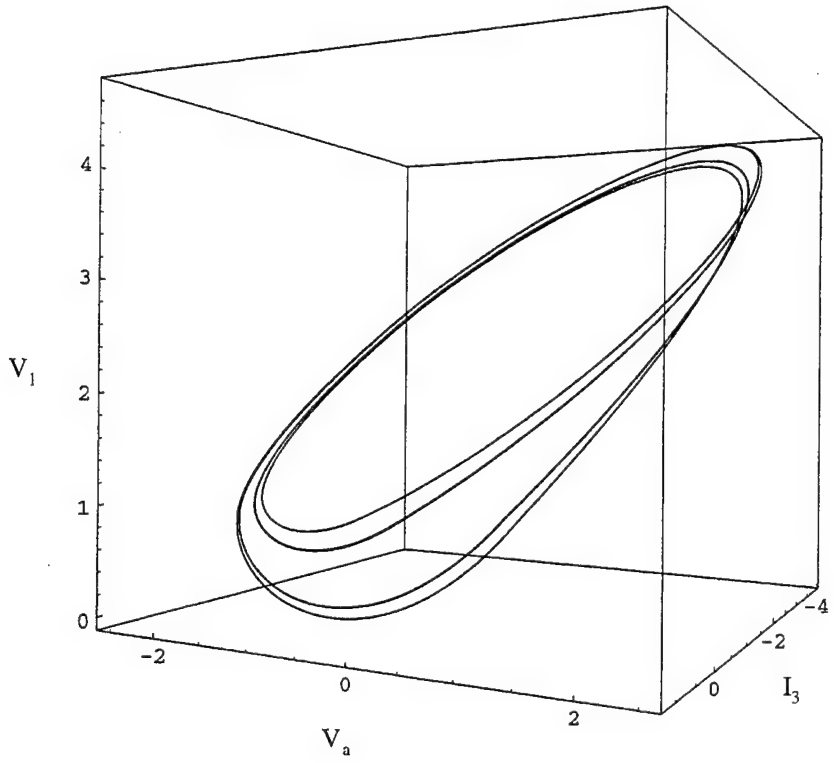

(a) Three-dimensional phase space plot of antenna voltage versus V_1 and I_3. Circuit parameters are R_0 = 12.5 Ω, L = 18.0 mH, C_1 = 10.0 nF, C_2 = 100.0 nF, G_a = -757.576 μS, G_b = -409.090 μS, E = 1.0 V, C_a = 10.0 pF, G = 539.0 μS.

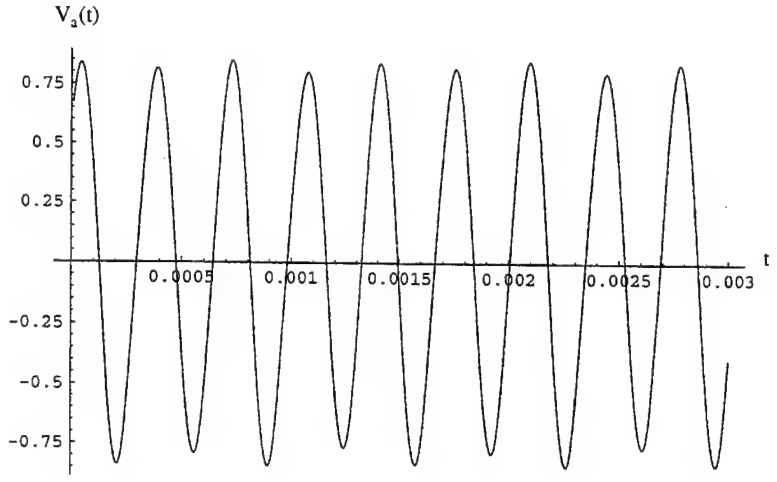

(b) Time series plot of antenna voltage versus time (same circuit parameters as Figure 7a).

FIGURE 7. Plot of Antenna Voltage Showing Period-4 Behavior.

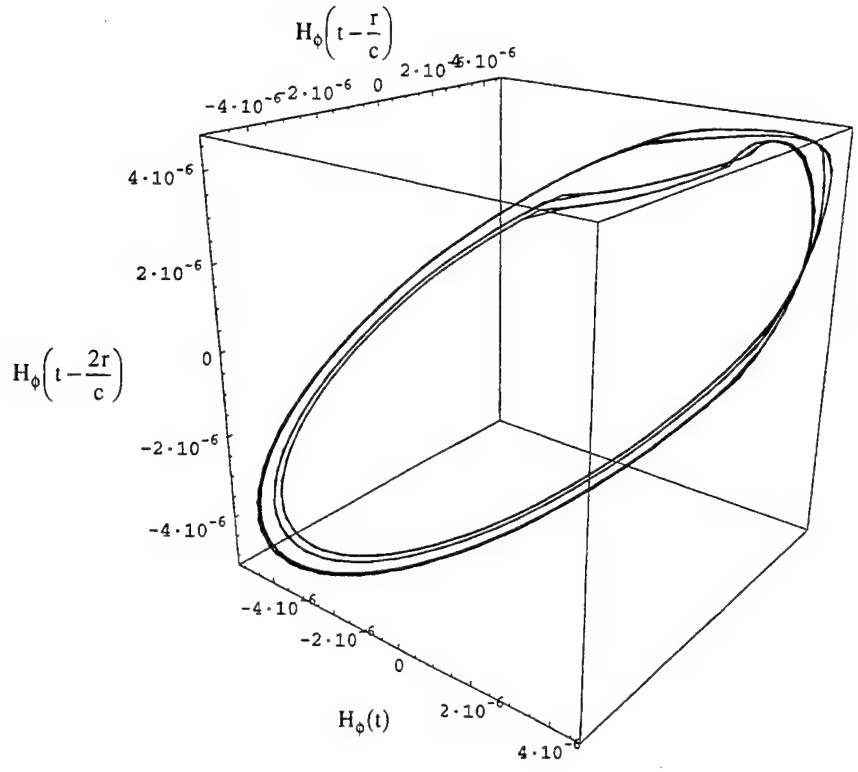

(a) Three-dimensional delay coordinate plot of magnetic field, H_ϕ. Circuit parameters are $R_0 = 12.5\ \Omega$, $L = 18.0$ mH, $C_1 = 10.0$ nF, $C_2 = 100.0$ nF, $G_a = -757.576\ \mu$S, $G_b = -409.090\ \mu$S, $E = 1.0$ V, $C_a = 10.0$ pF, $G = 539.0\ \mu$S, $r = 7.5 \times 10^3$ m, $h = 0.01$ m, $\theta = \pi/2$, $I_a = 100$ A, $c = 3 \times 10^8$ m/s.

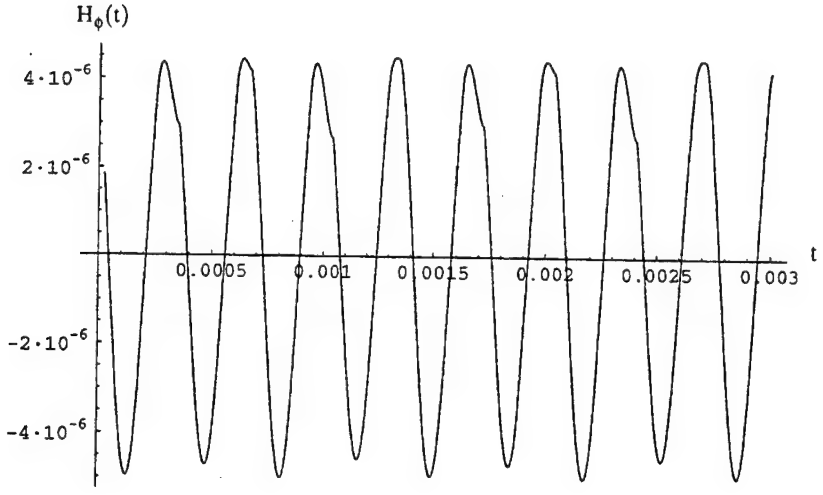

(b) Time series plot of magnetic field versus time (same parameters as Figure 8a).

FIGURE 8. Plot of Magnetic Field Showing Period-4 Behavior.

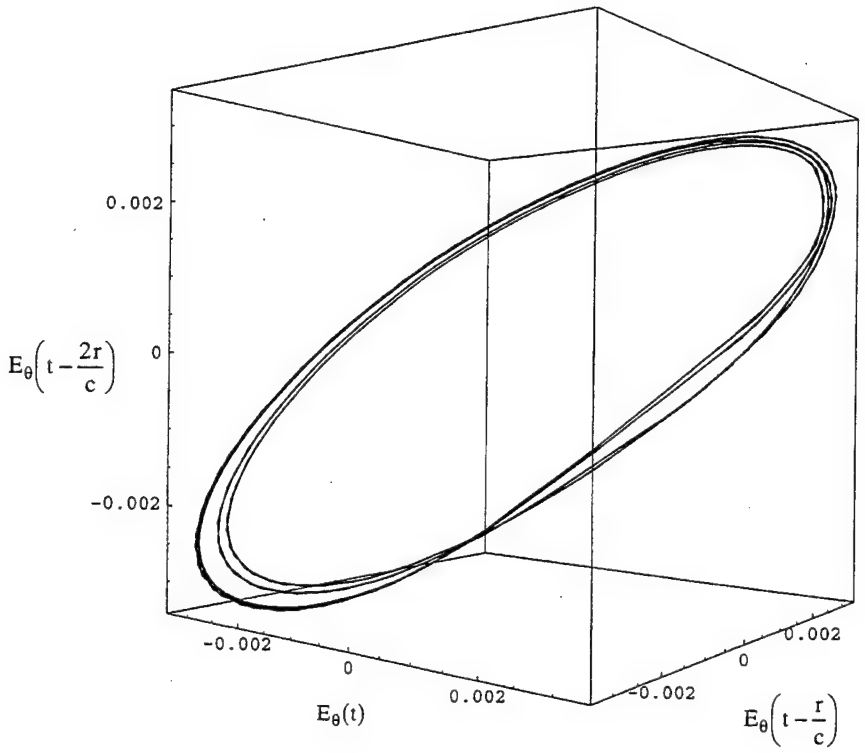

(a) Three-dimensional delay coordinate plot of electric field, E_θ (same parameters as Figure 8a).

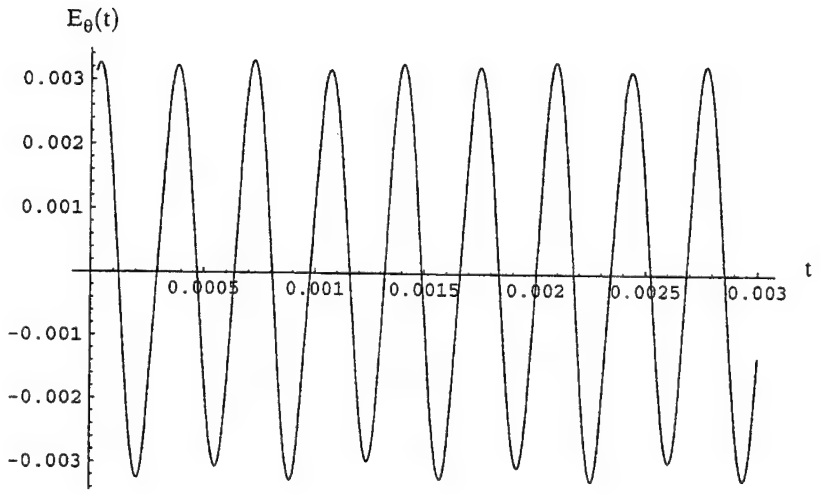

(b) Time series plot of electric field versus time (same parameters as Figure 8a).

FIGURE 9. Plot of Electric Field Showing Period-4 Behavior.

CASE 3: CHAOTIC CASE

The third case assumes that the circuit parameters of the equivalent circuit of Figure 3 are the same as for the two previous cases, except that now the conductance has been increased to 550 μS (Reference 19). This particular value of G causes the antenna voltage, $V_a(t')$, to be chaotic, specifically resulting in a spiral Chua's chaotic attractor (Reference 19). It is shown in Figure 10a and is an extremely distinctive chaotic attractor. Figure 10b is the associated time series plot of the antenna voltage amplitude as a function of time, which immediately shows complex, bounded, nonperiodic behavior.

Figure 11a is the three-dimensional delay plot of the magnetic field, H_ϕ. While again showing different amplitude, shape, and orientation when compared to Figure 10a, it exhibits the same spiral chaotic attractor form, including the central loop that overlaps the remainder of the spiral, with the remaining overlapping loops occurring at the top of the figure rather than at the bottom. A comparison of Figure 10b and Figure 11b shows similar behavior in the time series plots. Figure 12a, the delay plot of E_θ, also gives a very faithful representation of the spiral Chua's chaotic attractor, again showing the same overlapping loops as in Figure 10a in somewhat different orientations but distinctively seen. The time series plot of E_θ in Figure 12b is almost identical in form to the time series antenna voltage plot in Figure 10b.

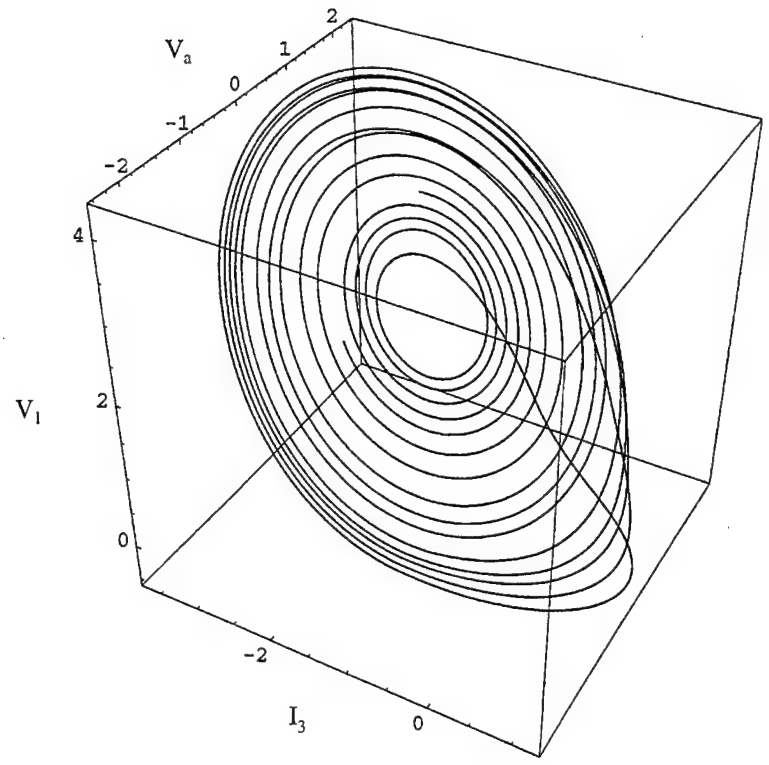

(a) Three-dimensional phase space plot of antenna voltage versus V_1 and I_3. Circuit parameters are R_0 = 12.5 Ω, L = 18.0 mH, C_1 = 10.0 nF, C_2 = 100.0 nF, G_a = -757.576 μS, G_b = -409.090 μS, E = 1.0 V, C_a = 10.0 pF, G = 550.0 μS.

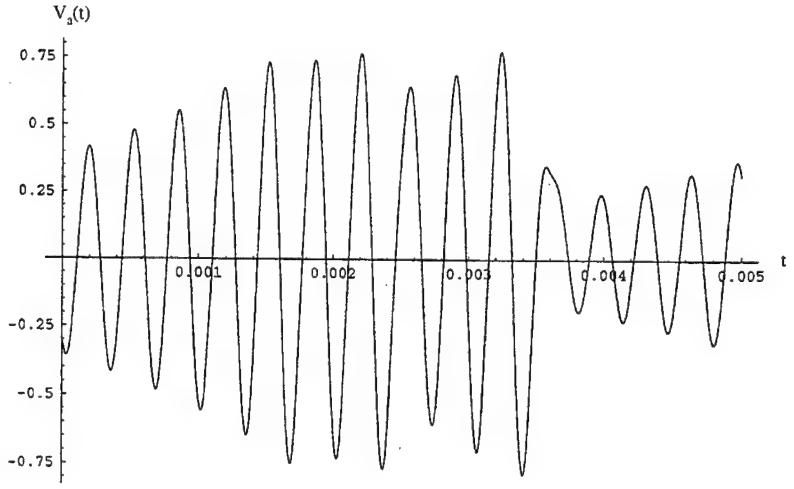

(b) Time series plot of antenna voltage versus time showing complex nonperiodic behavior (same circuit parameters as Figure 10a).

FIGURE 10. Plot of Antenna Voltage Showing Chaotic Behavior.

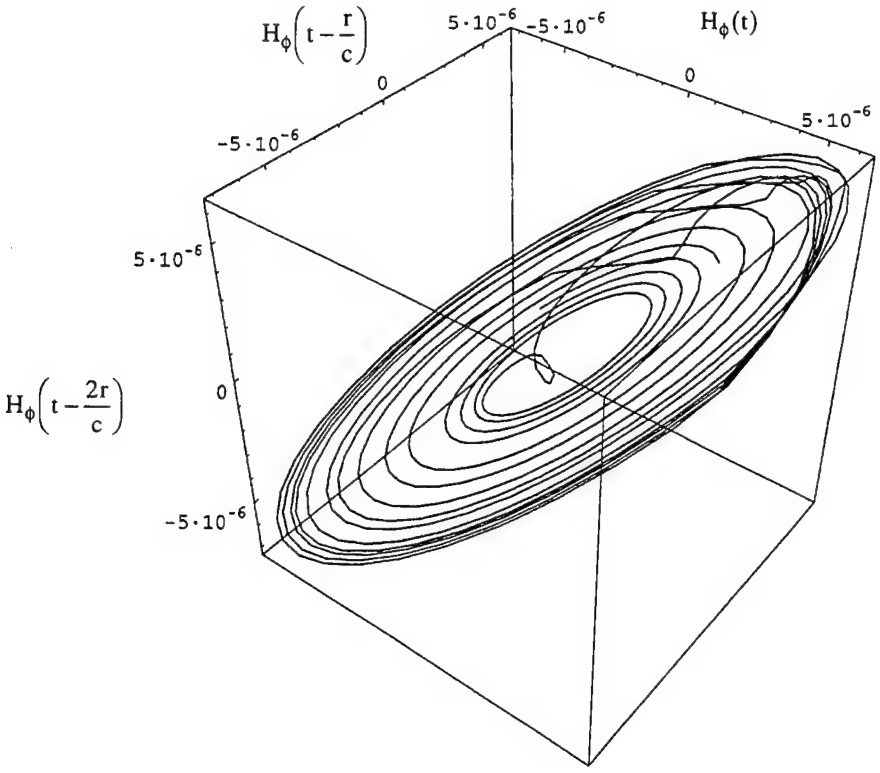

(a) Three-dimensional delay coordinate plot of magnetic field, H_ϕ. Circuit parameters are $R_0 = 12.5\ \Omega$, $L = 18.0$ mH, $C_1 = 10.0$ nF, $C_2 = 100.0$ nF, $G_a = -757.576\ \mu S$, $G_b = -409.090\ \mu S$, $E = 1.0$ V, $C_a = 10.0$ pF, $G = 550.0\ \mu S$, $r = 7.5 \times 10^3$ m, $h = .01$ m, $\theta = \pi/2$, $I_a = 100$ A, $c = 3 \times 10^8$ m/s.

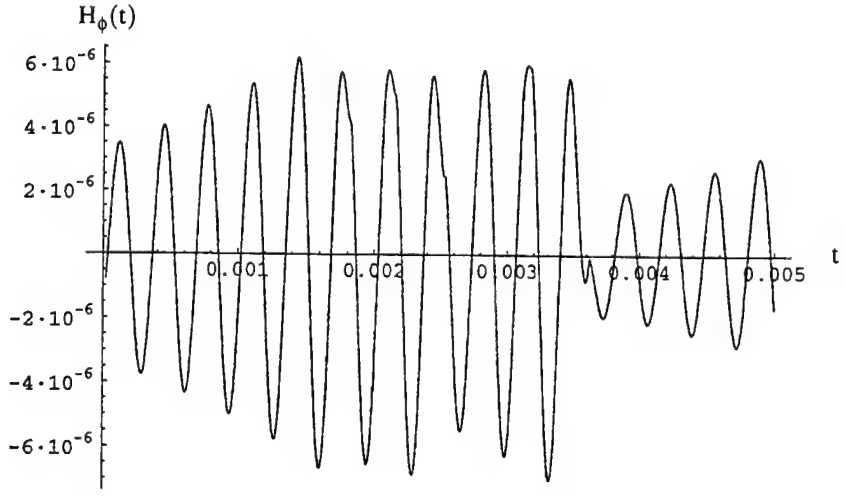

(b) Time series plot of magnetic field versus time showing complex nonperiodic behavior (same parameters as Figure 11a).

FIGURE 11. Plot of Magnetic Field Showing Chaotic Behavior.

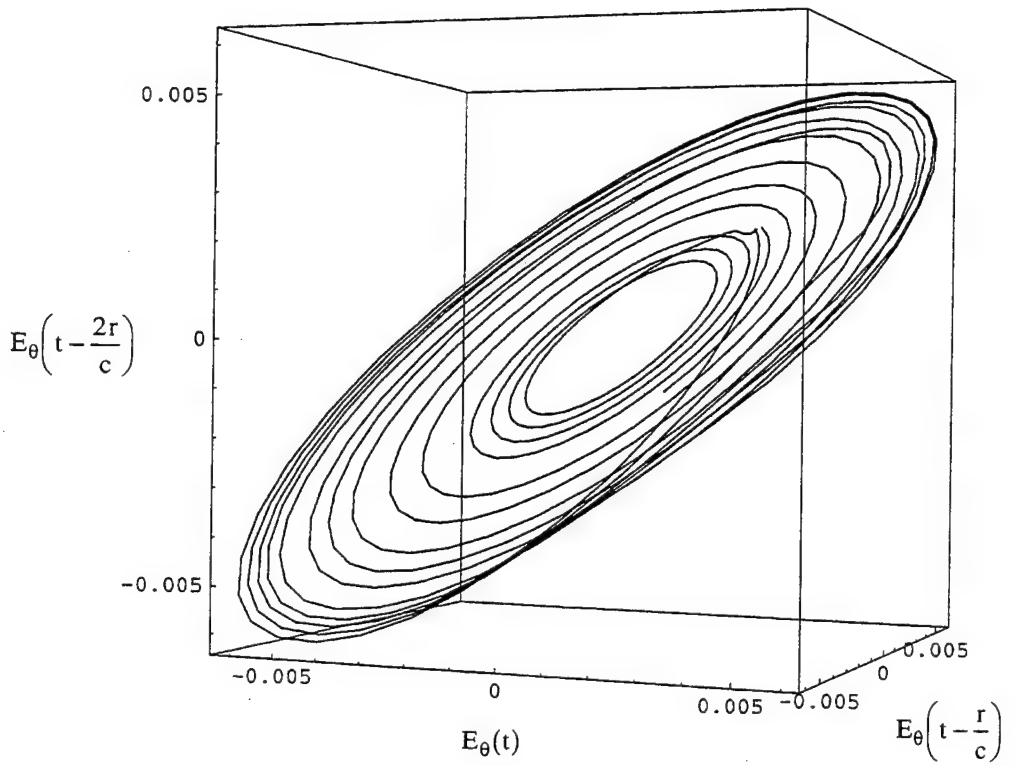

(a) Three-dimensional delay coordinate plot of electric field, E_θ (same parameters as Figure 11a).

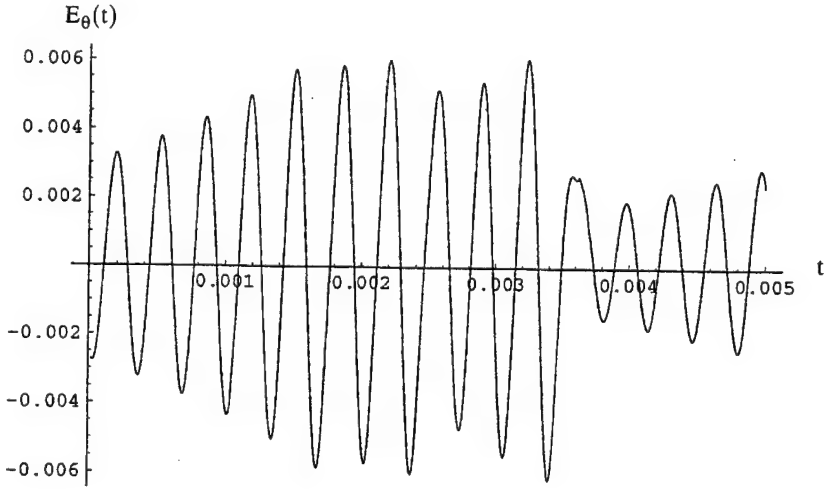

(b) Time series plot of electric field versus time showing complex, nonperiodic behavior (same parameters as Figure 11a).

FIGURE 12. Plot of Electric Field Showing Chaotic Behavior.

4. CONCLUSION

The electrically small dipole antenna loaded with Chua's oscillator as the nonlinear load was analyzed. By using certain numerical values for the linear reactive and resistive elements of this circuit, various types of periodic, period-doubled, and chaotic behavior that occur for the voltage at the antenna input terminals can also be shown to occur for the associated radiated electromagnetic field components. Using three cases, i.e., periodic, period-4, and chaotic behavior, we show that the voltage characteristic dynamics determined at the input terminals are the same dynamics of the radiated electromagnetic field components.

Thus, for an electrically small dipole, we demonstrated that when the antenna voltage function is temporally chaotic, the antenna will radiate temporally chaotic electromagnetic fields with the same dynamical behavior referenced to some later time. Similarly, when the antenna voltage is periodic, the radiated fields will be periodically referenced to some later time also. Thus, switching between a periodic and a chaotic temporal electromagnetic field behavior can be accomplished by simply increasing the conductance of a single resistor of the antenna/Chua's oscillator equivalent circuit.

REFERENCES

1. M. Kanda. "Analytical and Numerical Techniques for Analyzing an Electrically Short Dipole With a Nonlinear Load," *IEEE Trans. Antennas Propagation*, AP-28 (January 1980), pp. 71-78.

2. J. A. Landt, E. K. Miller, and F. J. Deadrick. "Time Domain Modeling of Nonlinear Loads," *IEEE Trans. Antennas Propag.*, AP-31 (January 1983), pp. 121-126.

3. T. K. Liu and F. M. Tesche. "Analysis of Antennas and Scatterers With Nonlinear Loads," *IEEE Trans. Antennas Propag.*, AP-24 (March 1976), pp. 131-139.

4. T. K. Sarkar and D. D. Weiner. "Scattering Analysis of Nonlinearly Loaded Antennas," *IEEE Trans. Antennas Propag.*, AP-24 (March 1976), pp. 125-131.

5. H. Schuman. "Time Domain Scattering From a Nonlinearly Loaded Wire," *IEEE Trans. Antennas Propag.*, AP-22 (July 1974), pp. 611-613.

6. M. Kanda. "The Time-Domain Characteristics of a Traveling-Wave Linear Antenna With Linear and Nonlinear Parallel Loads," *IEEE Trans. Antennas Propag.*, AP-28 (March 1980), pp. 267-276.

7. J. A. Landt. "Network Loading of Thin-Wire Antennas and Scatterers in the Time Domain," *Radio Sci.,* Vol. 16 (November/December 1981), pp. 1241-1247.

8. R. Janaswamy and S-W. Lee. "Scattering From Dipoles Loaded With Diodes," *IEEE Trans. Antennas Propag.*, Vol. AP-36 (November 1988), pp. 1649-1651.

9. J. A. Landt. "Effects of Nonlinear Loads on Antennas and Scatterers," presented at the AGARD Lecture Series No. 131, The Performance of Antennas in Their Operational Environment, Ankara, Turkey, 19-20 October 1983. Paper UNCLASSIFIED. Published Neuilly-sur-Seine, France, AGARD, 1983. Publication UNCLASSIFIED.

10. A. N. Yegorov and Ye. V. Ryabtsev. "Electrodynamic Analysis of Nonstationary Processes in Thin Cylindrical Antennas With Nonlinear Loads," *Radiotekh. Elektron.*, Vol. 33, No. 12 (1988), pp. 2471-2482.

11. Ya. S. Shifrin, A. I. Luchaninov, and A. A. Shcherbina. "Nonlinear Antenna Effects," *Izv. Vyssh. Uchebn. Zaved. Radiotekh. Elektron.*, Vol. 33, No. 2 (1990), pp. 4-13.

12. L. O. Chua. "Nonlinear Circuits," *IEEE Trans. Circuits Syst.*, Vol. CAS-31 (January 1984), pp. 69-87.

13. T. Matsumoto. "A Chaotic Attractor From Chua's Circuit," *IEEE Trans. Circuits Syst.*, Vol. CAS-31 (1984), pp. 1055-1058.

14. L. O. Chua, M. Komura, and T. Matsumoto. "The Double Scroll Family, Parts I and II," *IEEE Trans. Circuits Syst.*, Vol. CAS-33 (November 1986), pp. 1073-1118.

15. L. O. Chua. "The Genesis of Chua's Circuit," *Archiv. fur Electronik und Ubertragungstechnik*, Vol. 46, No. 4 (1992), pp. 250-257.

16. M. P. Kennedy. "Three Steps to Chaos—Part I: Evolution," *IEEE Trans. Circuits Syst.*, Vol. CAS-40 (October 1993), pp. 640-656.

17. M. P. Kennedy. "Three Steps to Chaos—Part II: A Chua's Circuit Primer," *IEEE Trans. Circuits Syst.*, Vol. CAS-40 (October 1993), pp. 657-674.

18. M. P. Kennedy. "Robust Op Amp Realization of Chua's Circuit," *Frequenz*, Vol. 46 (March/April 1992).

19. M. P. Kennedy. "ABC (Adventures in Bifurcations and Chaos): A Program for Studying Chaos," *J. Franklin Inst.*, Vol. 331B, No. 6 (1994), pp. 631-658.

20. T. S. Parker and L. O. Chua. *Practical Numerical Algorithms for Chaotic Systems*. New York, Springer-Verlag, 1989.

21. R. Hilborn. *Chaos and Nonlinear Dynamics*. New York, Oxford, 1994.

22. K. T. Alligood, T. D. Sauer, and J. A. Yorke. CHAOS: *An Introduction to Dynamical Systems*. New York, Springer-Verlag, 1997.

INITIAL DISTRIBUTION

2 Naval Air Warfare Center Weapons Division, Point Mugu
  Code 474500E, D. Hilliard (1)
  Code 452100E, J. Hurley (1)
1 Naval War College, Newport (1E22, President)
1 Headquarters, 497 IG/INTW, Falls Church (OUWG Chairman)
2 Defense Technical Information Center, Fort Belvoir
1 Center for Naval Analyses, Alexandria, VA (Technical Library)

ON-SITE DISTRIBUTION

4 Code 4TL000D (3 plus Archives copy)
1 Code 4T4100D, Decker
2 Code 4T4110D
  Bowling (1)
  Chesnut (1)
11 Code 4T4120D
  DeSandre (1)
  Marrs (1)
  Overfelt (8)
  Yoo (1)
1 Code 411000D, Keeter
6 Code 452310D
  Frisbee (1)
  Schramm (1)
  Katzenstein (1)
  Otto (1)
  Roush (1)
  Wang (1)
1 Code 473000D, Hoppus
3 Code 473100D
  Chew (1)
  Kerns (1)
  Skatvold (1)
3 Code 473200D
  Afendyqiw (1)
  Ghaleb (1)
  Kidner (1)
4 Code 473300D
  Bling (1)
  Miller (1)
  Paolino (1)
  Schiefen (1)
1 Code 473400D, Neel